The pressure dependence of many-body interactions in the organic superconductor κ-(BEDT-TTF)$_2$Cu(SCN)$_2$ (BEDT-TTF ≡ bis(ethylene-dithio)tetrathiafulvalene): a comparison of high-pressure infrared reflectivity and Raman scattering experiments

2003 J. Phys.: Condens. Matter 15 5315

(http://iopscience.iop.org/0953-8984/15/30/313)

INSTITUTE OF PHYSICS PUBLISHING JOURNAL OF PHYSICS: CONDENSED MATTER

J. Phys.: Condens. Matter **15** (2003) 5315–5332 PII: S0953-8984(03)63148-6

The pressure dependence of many-body interactions in the organic superconductor κ-(BEDT-TTF)$_2$Cu(SCN)$_2$ (BEDT-TTF $\equiv$ bis(ethylene-dithio)tetrathiafulvalene): a comparison of high-pressure infrared reflectivity and Raman scattering experiments

R D McDonald[1,2], A-K Klehe[2], J Singleton[1,2] and W Hayes[2]

[1] NHMFL, Los Alamos National Laboratory, MS-E536, NM 87545, USA
[2] Clarendon Laboratory, Department of Physics, Parks Road, Oxford OX1 3PU, UK

E-mail: rmcd@lanl.gov

Received 8 May 2003
Published 18 July 2003
Online at stacks.iop.org/JPhysCM/15/5315

Abstract

We determine the pressure dependence of the electron–phonon coupling in κ-(BEDT-TTF)$_2$Cu(SCN)$_2$ by comparison of high-pressure Raman scattering and high-pressure infrared (IR) reflectivity measurements. The Raman active molecular vibrations of the BEDT-TTF dimers stiffen by 0.1–1% GPa^{-1}. In contrast, the corresponding modes in the IR spectrum are observed at lower frequency, with a pressure dependence of 0.5–5.5% GPa^{-1}, due to the influence of the electron–phonon interaction. Both dimer charge-oscillation and phase-phonon models are employed to extract the pressure dependence of the electron–molecular vibration coupling for these modes. Analysis of our data suggests that the reduction of electron–phonon coupling under pressure does not account for the previously observed suppression of superconductivity under pressure and that electron–electron interactions may contribute significantly to the pairing mechanism.

(Some figures in this article are in colour only in the electronic version)

1. Introduction

κ-(BEDT-TTF)$_2$Cu(SCN)$_2$ is one of the best characterized organic superconductors [1]. It is a highly anisotropic material with a quasi-two-dimensional band structure, whose Fermi surface topology has been determined by magnetotransport experiments [1, 2]. At ambient pressure κ-(BEDT-TTF)$_2$Cu(SCN)$_2$ is a superconductor with a transition temperature of $T_c \simeq 10.4$ K. T_c decreases upon the application of pressure until, at pressures P exceeding

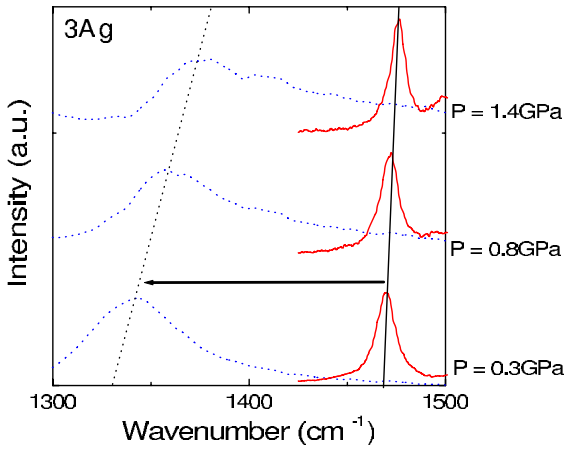

Figure 1. The spectral region containing the $3A_g$ molecular vibration, showing Raman spectra (solid curves) and IR spectra with polarization parallel to the crystallographic *b*-axis (dotted curves), for a selection of pressures at room temperature. The spectra are offset for clarity and the lines are a guide to the eye. Note the substantial softening effect of the increased electron–phonon interaction on the IR spectra with respect to the Raman spectra.

0.5 GPa, superconductivity is fully suppressed [2–4]. The quasiparticle effective mass, m^*, derived from magnetic quantum oscillation measurements, decreases linearly with pressure up to 0.5 GPa; above this pressure the magnitude of $\mathrm{d}m^*/\mathrm{d}P$ is strongly reduced [2]. The effective mass measured in this fashion includes contributions from both electron–phonon and electron–electron interactions [5].

In contrast, the optical mass, m_{opt}, extracted from a sum over the optical conductivity, decreases approximately linearly throughout the above pressure range [6]. This mass is thought to be dominated by intraband electronic processes, reflecting the band mass without renormalization by electron–electron and electron–phonon interactions [5][3]. The coincidence of a 'kink' in the pressure dependence of m^* with the pressure above which superconductivity is suppressed and the absence of a 'kink' in the pressure dependence of m_{opt} suggests that the interactions parameterized by m^* may be associated with the superconductivity.

The key question to address is the effect of these interactions, i.e. what is the dominant pairing mechanism for superconductivity in this material? In this paper we compare infrared (IR) [6][4] and Raman scattering [7] measurements under pressure to determine the role of the electron–phonon interaction. This is possible because the IR measurement probes the molecular vibrations dressed by the electron–phonon interaction [8, 9], whereas non-resonant Raman measurements probe the bare mode frequencies [8, 10]. The primary effect of the electron–phonon interaction is to soften the IR modes with respect to the Raman modes, as illustrated in figure 1.

There are two approaches to modelling the electron–molecular vibration coupling interaction and associated mode softening in organic charge transfer systems, the 'phase-phonon' theory and the 'dimer charge-oscillation' model. The phase-phonon theory approaches the problem from an electron band approximation where the charge carriers are

[3] In this paper we extract an effective mass from the optical data that is strongly influenced by interband electronic processes. We argue that in contrast to the intraband processes the interband ones are renormalized by quasi-particle interactions; see section 4.1.

[4] Polarized IR reflectance measurements were performed in the highly conductive, crystallographic *bc*-plane of the crystal with the electric field polarized parallel to the crystallographic *b*- or crystallographic *c*-axis.

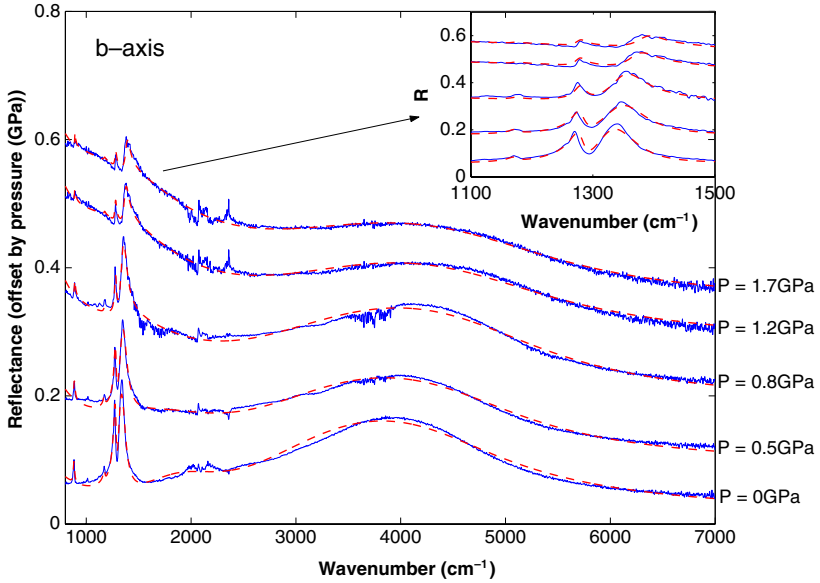

Figure 2. The room temperature diamond/sample IR reflectance offset by pressure for polarization parallel to the *b*-axis. The measurement (solid curves) and the phase-phonon fit (dashed curves). The inset magnifies the spectral region containing the C=C mode.

naturally delocalized. The alternative dimer charge-oscillation theory is formulated in real space such that the electronic behaviour is implicitly localized. In reality the electronic properties of κ-(BEDT-TTF)$_2$Cu(SCN)$_2$ are somewhere between the extremes of a localized and an itinerant system [1]. For this reason we apply both the dimer charge-oscillation and phase-phonon models to analyse the data.

This paper is organized as follows. In section 2 we describe the vibrational spectra of κ-(BEDT-TTF)$_2$Cu(SCN)$_2$ as observed by means of both non-resonant Raman scattering and polarized IR reflectivity. Section 3 describes the methods of analysis, specifically how the pressure dependence of the electron–phonon coupling is extracted. The first subsection of the discussion, section 4.1, contains a comparison of the quasiparticle masses that result from the different methods of analysis. Subsequently, in section 4.2, in the light of the pressure dependence of the electron–phonon coupling, the implications for the superconducting pairing mechanism are discussed. Conclusions and a summary are given in section 5.

2. Description of the observed vibrational modes

Four modes are observed in both the high-pressure room temperature Raman and IR spectra (see figures 2 and 3 and table 1). They are labelled with subscripts indicating the atoms/bond predominantly involved in the vibration [11]. In order of increasing frequency they are the C–S mode originating from the BEDT-TTF 60B$_{3g}$ asymmetric vibration, the central C=C mode originating from the BEDT-TTF 3A$_g$ symmetric vibration and two Cu(SCN)$_2$ anion modes. Determining the pressure dependence of the central C=C mode in the IR spectrum is not straightforward due to the overlap of several modes with varying pressure dependences. In a recent publication [12], IR spectra from the deuterated salt have been used to model this Fermi resonance and extract the linear pressure dependence of the overlapping modes (the central

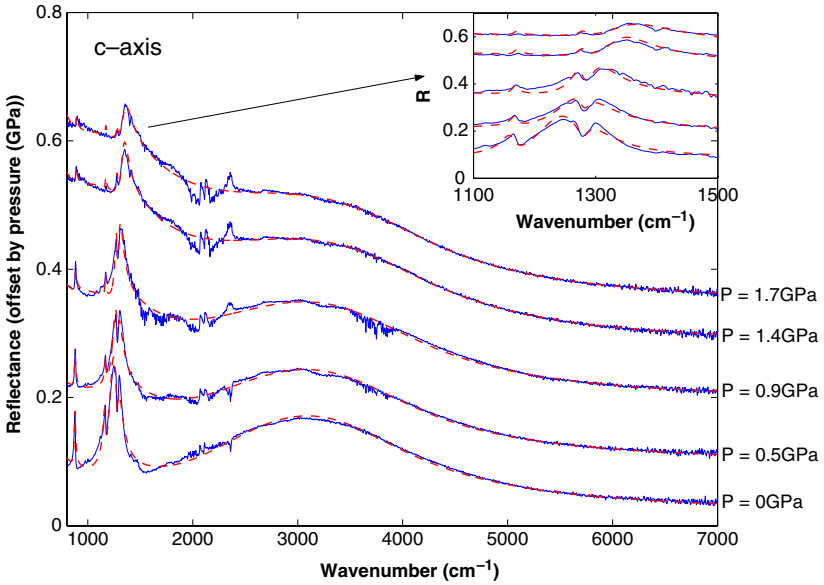

Figure 3. The room temperature diamond/sample IR reflectance offset by pressure for polarization parallel to the *c*-axis. The measurement (solid curves) and the phase-phonon fit (dashed curves). The inset magnifies the spectral region containing the C=C mode.

Table 1. Raman and IR frequencies and pressure shifts taken from [6, 7, 12].

		Raman		Infrared *b*-axis		Infrared *c*-axis	
Mode	Assignment [11]	(cm^{-1})	+(% GPa^{-1})	(cm^{-1})	+(% GPa^{-1})	(cm^{-1})	+(% GPa^{-1})
ω_{CT}	—	—	—	2910	+4.0	2390	+4.0
ω_{CS}	B_{3g}	886.2	+0.85	883.5	+0.71	873.6	+1.0
ω_{CC}	A_g	1467.7	+0.4	1290	+2.5	1210	+5.5
ω_{CH_1}	B_{3u}	—	—	1181	+0.5	1177	+0.5
ω_{CH_2}	B_{1u}	—	—	1290	+0.5	1281	+0.5
ω_{anion1}	CN	2064.6	+0.1	2067.4	+0.1	2065.6	+0.15
ω_{anion2}	CN	2106.3	+0.2	—	—	2109.3	+0.2

C=C mode and two C–H modes). The IR and Raman frequencies and the first-order pressure dependence of all modes discussed here are given in table 1.

The $Cu(SCN)_2$ anion modes do not exhibit any evidence of electron–phonon coupling, i.e. the difference between the IR and Raman frequencies for the anion modes is accounted for by purely vibrational coupling [7]. The zone centre frequency separation, $\Delta\omega_s$, between the symmetric (Raman active) and antisymmetric (IR active) combinations of the molecular vibrations is determined by the frequency of the optical branch of the lattice modes [7, 13]. The larger observed $\Delta\omega_s$ for the anion mode in the *b*-axis response, for which the lattice mode is stiffer (see table 1), is a further confirmation of the lattice mode assignment given in [7][5].

[5] The mode assignment that we confirm here corresponds to the experimental conditions of room temperature and high pressure, where only three lattice modes are observed; i.e. at room temperature and high pressure (unlike low temperature and ambient pressure) the intramolecular and intermolecular vibrational degrees of freedom do not appear to mix, so the intermolecular modes involve the molecules moving as a rigid unit with only one mode for each crystallographic direction.

3. Analysis

Electron–molecular vibration coupling can be characterized by a set of linear coupling constants, g_α, which parameterize the interaction between the αth normal mode, of frequency ω_α, and the molecular orbital in which the radical electron or hole resides [14]. For a donor molecule, g_α is the rate of change of the energy of the highest occupied molecular orbital with respect to the normal mode coordinate, Q_α [14]:

$$g_\alpha = \frac{\partial E}{\partial Q_\alpha}. \tag{1}$$

To obtain these coupling constants experimentally, an appropriate model has to be applied to the data. Two alternative approaches exist in the literature: the 'phase-phonon' theory and the 'dimer charge-oscillation' model. Both theories were initially developed by Rice [10, 15] to model the IR spectrum of semiconducting organic charge transfer systems. However, they have also been applied to a range of reduced dimensionality organic charge transfer salts, including metallic systems [8, 14, 16–20].

The phase-phonon theory approaches the problem from an electron band approximation where the charge carriers are naturally delocalized. A potential disadvantage of this approach is that it is a one-electron theory, i.e. all electron–electron correlation effects have to be included within an effective mass approximation [14].

The alternative dimer charge-oscillation theory is formulated in real space but is limited to a finite number of molecules. The IR response of the system is calculated from a superposition of the isolated units with no significant charge transfer between the units. For κ-phase BEDT-TTF salts the approximation is that the charge carriers are predominantly localized on the dimers which are weakly interacting with each other. Although this implies an insulating system, with the response of delocalized charge carriers parameterized separately, electron–electron correlations such as the on-site Coulomb repulsion can be included explicitly [17].

3.1. The dimer charge-oscillation model

This subsection outlines the derivation of the dimer charge-oscillation model [10, 17]. Not only does this aid discussion relating to the validity of applying this model to κ-(BEDT-TTF)$_2$Cu(SCN)$_2$, but it also lends theoretical weight to the concept of electron coupling to the antisymmetric combinations of molecular vibrations and not to the symmetric combinations. This concept is the key to comparing Raman and IR data in order to probe the electron–phonon coupling.

Each dimer unit is modelled by the following Hamiltonian ($\hbar = 1$) [10, 17]:

$$H = H_\mathrm{e} + H_\mathrm{v} + \sum_{\alpha,j} n_j g_\alpha Q_{\alpha,j}. \tag{2}$$

The first two terms describe, respectively, the electronic states and the molecular vibrations in the absence of vibrational coupling; j labels the molecule and α the normal mode of vibration. Rice's formulation includes only the totally symmetric (A_g) molecular modes. However, later theories have extended the theory to internal modes of other symmetries [21].

The electronic term, H_e, is of the form

$$H_\mathrm{e} = \sum_{j=1:2} E_0 n_j + V, \tag{3}$$

where $n_j = \sum_\sigma c^\dagger_{j,\sigma} c_{j,\sigma}$ is the occupation number operator for the molecular orbital of energy E_0. $c^\dagger_{j,\sigma}$ and $c_{j,\sigma}$ are the fermion creation and annihilation operators for an electron of spin σ [22, 23]. The exact form of the potential term, V, is arbitrary.

The phonon term, $H_{\rm v}$, is of the conventional form for a harmonic oscillator of frequency ω_α [17, 22, 23]:

$$H_{\rm v} = \sum_{j,\alpha} \omega_\alpha (b^\dagger_{j,\alpha} b_{j,\alpha} + \tfrac{1}{2}), \tag{4}$$

where $b^\dagger_{j,\alpha}$ and $b_{j,\alpha}$ are the boson creation and annihilation operators. Their sum is the displacement operator for the αth normal mode and their difference is the momentum operator [23], i.e.

$$Q_{j,\alpha} \propto (b^\dagger_{j,\alpha} + b_{j,\alpha}). \tag{5}$$

Because the dimer has been chosen as the base unit for this system, it is appropriate to introduce dimer mode coordinates

$$s_\alpha = \frac{1}{\sqrt{2}}(Q_{1,\alpha} + Q_{2,\alpha}) \tag{6}$$

and

$$q_\alpha = \frac{1}{\sqrt{2}}(Q_{1,\alpha} - Q_{2,\alpha}) \tag{7}$$

which are symmetric and antisymmetric combinations of the molecular mode coordinates respectively.

The third term in the Hamiltonian is a linear perturbation arising from the electron–molecular vibration coupling. Commutation of the dimer mode coordinates with the system Hamiltonian yields two equations of motion for the αth molecular mode [17, 24]:

$$\langle \ddot{s}_\alpha \rangle + \omega_\alpha^2 \langle s_\alpha \rangle = -\sqrt{2} g_\alpha \omega_\alpha \langle n_1 + n_2 \rangle \tag{8}$$

and

$$\langle \ddot{q}_\alpha \rangle + \omega_\alpha^2 \langle q_\alpha \rangle = -\sqrt{2} g_\alpha \omega_\alpha \langle n_1 - n_2 \rangle. \tag{9}$$

The right-hand side of the equation of motion for the symmetric combination of molecular modes is dependent on the total charge density, $\langle N_{\rm tot} \rangle = \langle n_1 + n_2 \rangle$, which for an isolated dimer is constant; i.e. the symmetric combination of modes is uncoupled from the electron system. Their unperturbed frequencies, ω_α, are therefore obtained experimentally from Raman scattering experiments [10].

The right-hand side of the equation of motion for the antisymmetric combination of molecular modes is dependent upon the electric dipole moment of the dimer, $\langle \boldsymbol{p} \rangle = \frac{1}{2} e \boldsymbol{a} \langle n_1 - n_2 \rangle$, where e is the electron charge and $\boldsymbol{a}$ is a vector perpendicular to the interface between the two molecules, whose magnitude is of the order of the intermolecular separation. Therefore the antisymmetric combination of modes is directly coupled to the electron dipole moment and is hence IR active [10]. For a simple two-state electron Hamiltonian these modes couple to the charge transfer excitation between the ground and excited states, $|1\rangle \rightarrow |2\rangle$.

Because the interaction part of the Hamiltonian is of the form

$$H_{\rm i} = \sum_k \rho_k \varphi_k, \tag{10}$$

where φ is a scalar potential, the expectation value of the operator ρ which characterizes the response of the system to the perturbation may be calculated using linear response theory [24–26]. The ground state expectation value of the Fourier components of the dipole moment, $\langle \boldsymbol{p}(\omega) \rangle$, and hence the complex conductivity, $\sigma(\omega)$, of the dimer charge-oscillation system are given by the linear response function [10, 24]:

$$\sigma(\omega) = -{\rm i}\omega \frac{e^2 \boldsymbol{a}^2}{2\mathcal{V}} \left(\frac{1}{\chi(\omega)} - \sum_\alpha \frac{g_\alpha^2 \omega_\alpha}{\omega_\alpha^2 - \omega^2 - {\rm i}\omega\gamma_\alpha} \right)^{-1}. \tag{11}$$

Here $\mathcal{V}$ is the molecular volume and $\chi(\omega)$ the reduced charge transfer polarizability;

$$\chi(\omega) = |\langle 2|\boldsymbol{p}|1\rangle|^2 \frac{2\omega_{\mathrm{CT}}}{\omega_{\mathrm{CT}}^2 - \omega^2 - \mathrm{i}\omega\Gamma}, \tag{12}$$

where $\langle 2|\boldsymbol{p}|1\rangle$ is the matrix element for the charge transfer transition of frequency ω_{CT}. The electron and phonon damping factors, Γ and γ_α, are introduced phenomenologically to account for the observed IR linewidths. It should be noted that this perturbation will alter the frequency at which the coupled molecular vibrations are observed in the IR spectrum; for $\omega_\alpha > \omega_{\mathrm{CT}}$ their frequencies will be red-shifted [17].

The crux of this subsection is to address how the dimer charge-oscillation model may be used to extract the electron–phonon coupling constants by means of experiment. Several approaches have been proposed to reduce the possible parameter space encountered when fitting IR reflectance data with this model. It has been noted [14] that the inverse of the real part of the conductivity, calculated using equation (11), consists of a constant background arising from the charge transfer band with peaks occurring at the unperturbed frequencies of the vibrational modes, ω_α. In principle, if this model accurately describes the data, Kramers–Kronig analysis could be used to calculate $\mathrm{Re}(1/\sigma(\omega))$ and thus determine the bare mode frequencies. However, because of uncertainties in applying the Kramers–Kronig procedure to reflectance from inside a diamond anvil pressure cell [6], Raman measurements of the unperturbed frequencies are more reliable.

Analysis of the poles and zeros of the response function (equation (11)) leads to the following approximate relation between the observed frequency of the IR phonon bands, Ω_α, their unperturbed frequencies, ω_α, the frequency of the coupling charge transfer band, ω_{CT}, and the dimensionless electron–molecular vibration coupling constants, λ_α [8, 18]:

$$\frac{\omega_\alpha^2 - \Omega_\alpha^2}{\omega_\alpha^2} = \lambda_\alpha \frac{\omega_{\mathrm{CT}}^2}{\omega_{\mathrm{CT}}^2 - \omega_\alpha^2}. \tag{13}$$

This expression is valid if the bare frequencies of the modes are well separated from each other or if the λ_α are sufficiently small that each mode may be treated individually. For κ-(BEDT-TTF)$_2$Cu(SCN)$_2$ the two observed modes with a finite λ_α (the C=C and C–S modes) are well separated from each other. Note that the C=C mode overlaps with two C–H modes as discussed in section 2; however, the lack of spectral weight associated with the C–H modes [12] indicates that their electron–phonon coupling is negligible in this case. Within the dimer charge-oscillation model, λ_α is related to g_α via [27]

$$\lambda_\alpha = \frac{2g_\alpha^2}{\omega_\alpha \omega_{\mathrm{CT}}}. \tag{14}$$

3.2. The electron–phonon coupling constant and its pressure derivative derived from the dimer charge-oscillation model

Equation (13) is used to calculate an electron–phonon coupling constant, λ_α, for each mode from its Raman and IR frequencies, ω_α and Ω_α, given knowledge of the energy, ω_{CT}, of the coupling charge transfer band [8, 18] (see table 2). The dominant source of error in this calculation is due to the width of the charge transfer band. There also exists the possibility of coupling to two different charge transfer transitions. The C=C mode, being an antisymmetric combination of A_g molecular modes, couples to the intradimer charge transfer [21]. It has been calculated [21], however, that the antiphase combination of B_{3g} molecular modes couples to charge transfer perpendicular to the intradimer direction. This suggests that the C–S mode couples to transitions between the lower and upper branches of the same band, not interband

Table 2. Dimensionless electron–phonon coupling constants and their pressure derivatives calculated using the dimer charge-oscillation model. Note that in this table the subscript on ω refers to the mode and the subscript on λ to the polarization direction.

Mode	λ_b	$\mathrm{d}\ln\lambda_b/\mathrm{d}P$ (% GPa^{-1})	λ_c	$\mathrm{d}\ln\lambda_c/\mathrm{d}P$ (% GPa^{-1})
ω_{CS}	0.01(1)	47.9	0.02(1)	−11.1
ω_{CC}	0.17(1)	−11.9	0.20(1)	−17.3
ω_{anion1}	0	0	0	0
ω_{anion2}	—	—	0	0

electronic transitions. However, it should be noted that the electron–phonon coupling constants for the C–S mode have been calculated using the same ω_{CT} as the C=C mode because it is impossible to distinguish the contributions to the IR spectrum from different transitions.

The pressure derivative of equation (13),

$$\frac{\mathrm{d}\ln\lambda_\alpha}{\mathrm{d}P} = 2\frac{\Omega_\alpha^2}{\omega_\alpha^2-\Omega_\alpha^2}\left[\frac{\mathrm{d}\ln\omega_\alpha}{\mathrm{d}P}-\frac{\mathrm{d}\ln\Omega_\alpha}{\mathrm{d}P}\right]+2\frac{\omega_\alpha^2}{\omega_{\mathrm{CT}}^2-\omega_\alpha^2}\left[\frac{\mathrm{d}\ln\omega_{\mathrm{CT}}}{\mathrm{d}P}-\frac{\mathrm{d}\ln\omega_\alpha}{\mathrm{d}P}\right], \tag{15}$$

has a weaker dependence on the value of ω_{CT}. However, the dominant source of error in equation (15) arises from the difficulty in determining an accurate pressure dependence of the broad charge transfer band. Fitting the IR reflectance data with a simple Drude–Lorentz model [6] provides an estimate for the pressure dependence of ω_{CT}. Using a value of $4 \pm 4\%$ GPa^{-1} for both *b*- and *c*-axes [6] results in an error in the pressure derivative of the coupling constant for the C=C mode of $\pm 3.5\%$ GPa^{-1} for the *b*-axis and $\pm 5\%$ GPa^{-1} for the *c*-axis. The error in the pressure derivative of the coupling constant for the C–S mode is larger (8% GPa^{-1} for the *b*-axis and 28% GPa^{-1} for the *c*-axis) because λ_{CS} is so small.

Because the dimer charge-oscillation model is formulated for a localized system, λ_α calculated in this manner parameterizes the strength of interaction between the phonons and the intradimer charge transfer. On the other hand, the electron–phonon coupling constant associated with phonon-mediated superconductivity parameterizes the strength of interaction between the phonons and the delocalized charge carriers. Therefore to use this model to draw any conclusions regarding the superconducting mechanism requires the assumption that the electron–phonon coupling for the intradimer charge transfer will, to first order, have the same pressure dependence as the electron–phonon coupling for the interdimer charge transfer. This assumption is reasonable because it is the same molecular orbitals that are responsible for intradimer and interdimer wavefunction overlap. At the Γ point (the long-wavelength limit), neighbouring dimers vibrate in phase [28] and, as a result, an antiphase combination of molecular vibrations that modulates the intradimer wavefunction overlap will also modulate the interdimer wavefunction overlap.

3.3. The phase-phonon model

Phase-phonon theory essentially describes the same phenomenon as the dimer charge-oscillation theory (see equation (2)). However, because it is formulated in reciprocal space the model is easily extended to metallic systems. This model is not just limited to the dimer unit, but attributes the IR activity of the coupled phonon modes to phase oscillations of the spatial charge density, induced by the electron–phonon interaction [15].

The system Hamiltonian is similar to that used in the dimer charge-oscillation theory, and includes an electronic term, H_{e}, a phonon term, H_{v}, and a linear coupling term, H_{i}:

$$H = H_{\rm e} + H_{\rm v} + \frac{1}{\sqrt{N}} \sum_{\alpha,q} g_\alpha Q_\alpha(q) \rho_{-q}. \tag{16}$$

The electronic term has essentially the same form as (3):

$$H_{\rm e} = \sum_{k,\sigma} E_k c^\dagger_{k,\sigma} c_{k,\sigma} + V(\rho_{q_0} + \rho_{-q_0}), \tag{17}$$

except that the operators create or annihilate a particle in a k-state, not at a real-space location, i.e. it describes a system of conduction electrons moving in a weak periodic potential, V, of wavevector q_0. The operator $\rho_q = \sum_k c^\dagger_{k+q} c_k$ creates an electronic density fluctuation of wavevector q.

The phonon term is identical to that used in the dimer charge model except the phonon operators also act on k-states. The electron–molecular vibration coupling is included as a linear perturbation, in this case linking the Fourier transform of the mode displacement vector, $Q_\alpha(q) \propto (b_\alpha(q) + b^\dagger_\alpha(-q))$, to an electronic density fluctuation of the same wavevector, q.

$$H_{\rm i} = \frac{1}{\sqrt{\mathcal{N}}} \sum_{\alpha,q,k} g_\alpha c^\dagger_{k+q} c_k (b_\alpha(q) + b^\dagger_\alpha(-q)) \tag{18}$$

where $\mathcal{N}$ is the density of conduction electrons.

For the case initially considered by Rice [15], $q_0 = 2k_{\rm F}$ (twice the Fermi wavevector), so the periodic potential induces the conduction electrons to condense into a charge-density-wave state. However, the derivation that follows is equally applicable to a metallic system. The frequency-dependent conductivity for an insulating system is due simply to interband electronic transitions [29],

$$\sigma(\omega) = \frac{\omega_{\rm p}^2}{{\rm i}\omega}[f(x) - f(0)], \tag{19}$$

where the plasma frequency, $\omega_{\rm p}$, parameterizes the band curvatures. $f(0) = 1$ and

$$f(x) = \frac{\left[{\rm i}\pi + \ln\left(\frac{1-S}{1+S}\right)\right]}{2Sx^2}, \tag{20}$$

where $S = \sqrt{1 - 1/x^2}$ and $x = \frac{\omega}{2\Delta_0}$ with Δ_0 equal to the band gap. Including the electron–phonon coupling modulates the on-site electron energy and hence the band gap, so $\Delta = \Delta_0 + \sum_\alpha \Delta_\alpha {\rm e}^{{\rm i}\phi_\alpha}$, where Δ_α and ϕ_α are the amplitude and phase respectively of the distortion potentials which are proportional to g_α. The single-electron contributions to $\sigma(\omega)$ are of the same form as in the uncoupled case but with $x = \frac{\omega}{2\Delta}$. In addition to the single-electron contributions there are collective contributions associated with oscillations in the phases, ϕ_α, of the combined lattice–charge distortions. Collective modes associated with oscillations in amplitude, Δ_α, also occur: however, they preserve dipole moment and hence do not contribute to the dielectric response [15, 19].

Including the collective mode contribution, the frequency-dependent conductivity is given by [15]

$$\sigma(\omega) = -\frac{\omega_{\rm p}^2}{{\rm i}\omega}[f(x) - f(0) - x^2 (f(x))^2 \lambda D_\phi(x)]. \tag{21}$$

D_ϕ is a phonon-like propagator for the phase oscillations given by

$$\frac{1}{D_\phi} = \frac{1}{D_0} + 1 - \frac{\Delta_0}{\Delta} + \lambda x^2 f(x). \tag{22}$$

D_0 is the same single-phonon propagator as is used in the dimer charge-oscillation model,

$$D_0 = -\sum_\alpha \frac{\lambda_\alpha}{\lambda} \frac{\omega_\alpha^2}{\omega_\alpha^2 - \omega^2 - {\rm i}\omega\gamma_\alpha}. \tag{23}$$

In the phase-phonon model the dimensionless coupling constant λ is related to g_α via

$$\lambda_\alpha = \frac{\mathcal{N}(k_F) g_\alpha^2}{\omega_\alpha}, \tag{24}$$

where $\mathcal{N}(k_F)$ is the density of electron states at the Fermi surface, and the total electron–phonon coupling constant $\lambda = \sum_\alpha \lambda_\alpha$ [14].

It is necessary to include an electronic damping term, Γ, to account for the finite electron lifetime if the model is to be applied to a metallic system, i.e. when a large plasma frequency is required to account for the intraband processes. In this case $f(x)$ is replaced by $f(x+i\Gamma)$ [30].

For $\omega_\alpha < 2\Delta$, decay of the collective mode via excitation of a real electron–hole pair is energetically impossible. As a result each mode contributes a sharp absorption band to the IR spectrum whose width is determined solely by the lineshape of the uncoupled phonon mode. For $\omega_\alpha > 2\Delta$ the collective modes become damped via electron–hole excitation, appearing as indentations in the electronic background [19].

3.4. The electron–phonon coupling constant and its pressure derivative derived from the phase-phonon model

The electron–phonon coupling constant that occurs in the phase-phonon model parameterizes the degree to which each molecular vibration modulates the energy of the electronic band structure, i.e. it parameterizes both the interband and intraband electron–phonon coupling.

To calculate λ_α for each mode, the full diamond/sample IR reflectance spectrum [6] is fitted at each pressure point. The model function for this fit consists of the phase-phonon model plus a high-frequency contribution to the dielectric constant, ε_∞, and a highly damped Lorentzian oscillator to account for the anomalous electronic damping at room temperature [6]. The plasma frequency, electronic damping and perturbed and unperturbed interband transition frequencies are treated as free parameters. As with a simple Drude response, the plasma frequency parameterizes the density of states and band curvature, but in this case the electronic damping controls the relative spectral weights of the interband and intraband processes.

Four phase-phonon collective modes ($\alpha = 1, \ldots, 4$) are used to model the spectrum, one for the C–S mode and three for the C=C mode and its Fermi resonance with the C–H modes. It was found that the lineshape of the Fermi resonance could be reproduced in an analogous manner to the Green function model used in [12], i.e. with one strongly coupled C=C mode and two C–H modes with negligible electron–phonon coupling (see the insets of figures 2 and 3). The pressure dependence of the modes' Raman frequencies and the pressure dependence of the dips from the Green function model were used to fix the frequency of the collective modes. Their damping and coupling strengths were left as free parameters, however.

In this model the degree of mode softening associated with the electron–phonon coupling is predominantly parameterized by the perturbation to the interband transition, i.e. the difference between the perturbed and unperturbed transition frequencies. The coupling strength, λ_α, controls the mode softening to a lesser extent, mainly parameterizing the spectral weight associated with each mode. Because of this, correctly determining λ relies on accurately modelling the background reflectance in the spectral region containing the modes. To this end, it was found that including the heavily damped Lorentzian to help model this material's anomalous Drude response drastically reduced the scatter in the λ-data. The three parameters describing the Lorentzian, ω_e, γ_e and $\Delta\varepsilon_e$, were also free.

[6] The electronic contributions to the spectra are not accurately reproduced using a single frequency-independent value for the electronic damping.

Table 3. Phase-phonon model parameters and their first-order pressure shifts.

	b-axis values		*c*-axis values	
Parameter	(cm^{-1})	+(% GPa^{-1})	(cm^{-1})	+(% GPa^{-1})
ω_p	(6816 ± 120)	$+(13 \pm 2)$	(5190 ± 66)	$+(19 \pm 2)$
Γ	(815 ± 16)	$+(45 \pm 3)$	(781 ± 12)	$+(45 \pm 3)$
Δ_0	(1132 ± 13)	$+(10 \pm 2)$	(743 ± 7)	$+(17 \pm 2)$
Δ	(1407 ± 14)	$+(6 \pm 2)$	(1064 ± 8)	$+(6 \pm 1)$
$\Delta - \Delta_0$	(275 ± 3)	$-(7 \pm 2)$	(320 ± 3)	$-(19 \pm 2)$
γ_{CS}	(15 ± 0.5)	$-(26 \pm 7)$	(13 ± 0.5)	$+(8 \pm 8)$
γ_{CC}	(68 ± 2)	$-(21 \pm 5)$	(101 ± 5)	$-(18 \pm 6)$
ω_e	(1905 ± 25)	$-(28 \pm 2)$	(1257 ± 21)	$-(12 \pm 2)$
γ_e	(1214 ± 51)	$+(2 \pm 6)$	(1065 ± 38)	$-(21 \pm 2)$
$\Delta\varepsilon_e$	(0.90 ± 0.15)	$+(388 \pm 22)$	(1.00 ± 0.10)	$+(272 \pm 15)$
ε_∞	(3.9 ± 0.1)	$+(11 \pm 3)$	(3.4 ± 0.1)	$+(18 \pm 3)$
λ_{CS}	$(3 \times 10^{-3} \pm 1 \times 10^{-4})$	$-(32 \pm 5)$	$(3 \times 10^{-3} \pm 1 \times 10^{-4})$	$-(25 \pm 4)$
λ_{CC}	(0.080 ± 0.002)	$-(55 \pm 4)$	(0.073 ± 0.002)	$-(44 \pm 3)$

The lineshape of the anion modes is most accurately reproduced using uncoupled Lorentzian oscillators. Owing to their lack of electron coupling and their limited contribution to the spectrum, parameters describing them were not included in this model. Figures 2 and 3 indicate the quality of the fits for a representative selection of pressures.

Manually fitting 31 spectra, each consisting of 3300 data points, with an expression containing 12 free parameters, for each polarization, is both immensely time consuming and subject to systematic human error. To avoid this, a batch fitting procedure was employed. It consists of accurately fitting a limited number of data sets to determine approximate trends for the free parameters. These are then used as the starting conditions for an automatic least-squares fitting procedure for all data sets. Each fit is then checked visually for acceptance of its parameters.

The value of the free parameters and their first-order pressure shifts extracted from figures 4 and 5 are contained in table 3. The differences in the values of the coupling constants, λ, obtained from the phase-phonon model (table 3) and the dimer charge-oscillation model (table 2) are predominantly due to the different values for the interband transition used in the calculations.

4. Discussion

As well as vibrational features, the room temperature IR spectrum of κ-(BEDT-TTF)$_2$ Cu(SCN)$_2$ contains broad electronic features; a heavily damped Drude-like response in the far infrared and a mid-infrared (MIR) 'hump'. Regarding the MIR 'hump', the literature only agrees to the extent that it originates from excitation across a gap in the electronic spectrum [20, 31, 32]. The simplest picture assigns it to a gap in the single-electron band structure [20]. This model is improved by including electron–electron interaction effects [31]. In this case the 'hump' originates from a combination of the single-electron band gap and the on-site correlation energy. Which is considered dominant, and which the perturbation, depends upon how correlated the system is believed to be. Analogously, inclusion of the electron–phonon interaction modifies the electronic spectrum. The phase-phonon model includes this explicitly as a relatively small perturbation to the band gap. In the limit of large

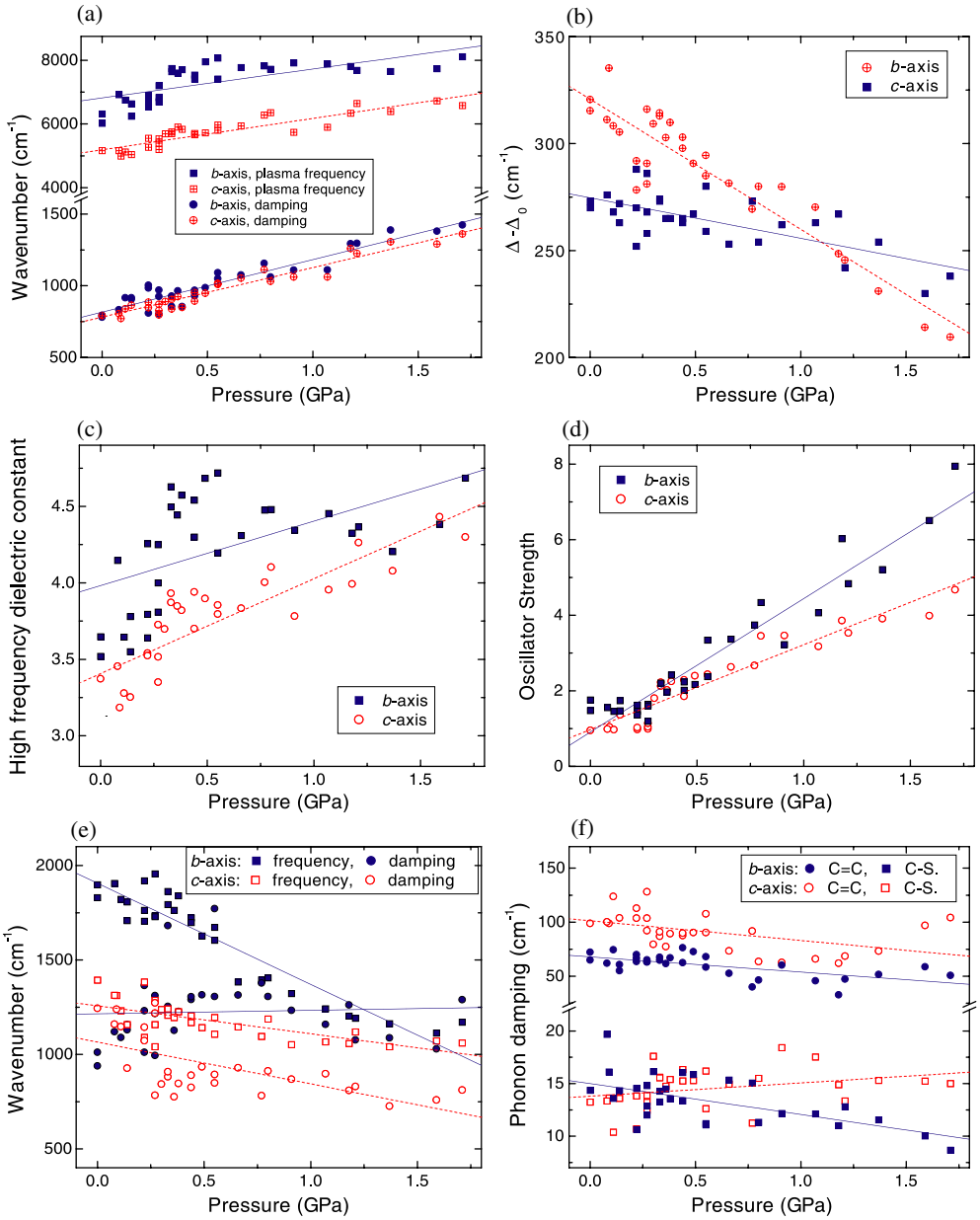

Figure 4. The pressure dependence of the free parameters of the phase-phonon model. Note that the linear fits indicate the first-order pressure dependence used for the batch fitting procedure. Solid lines and symbols are used for polarization parallel to the *b*-axis and dashed lines and hollow symbols for polarization parallel to the *c*-axis. (a) The plasma frequency and electronic damping. (b) The difference between the perturbed and unperturbed interband transition frequencies. (c) The high-frequency dielectric constant. (d) The strength of the Lorentzian oscillator. (e) The frequency and damping of the Lorentzian oscillator. (f) The damping of the C–S and C=C modes.

electron–phonon coupling, the strain field is considered to localize the charge carrier [32], in which case the small-polaron binding energy will be the band gap dressed by the electron–phonon interaction. All these theories share the common assumption that IR active interband

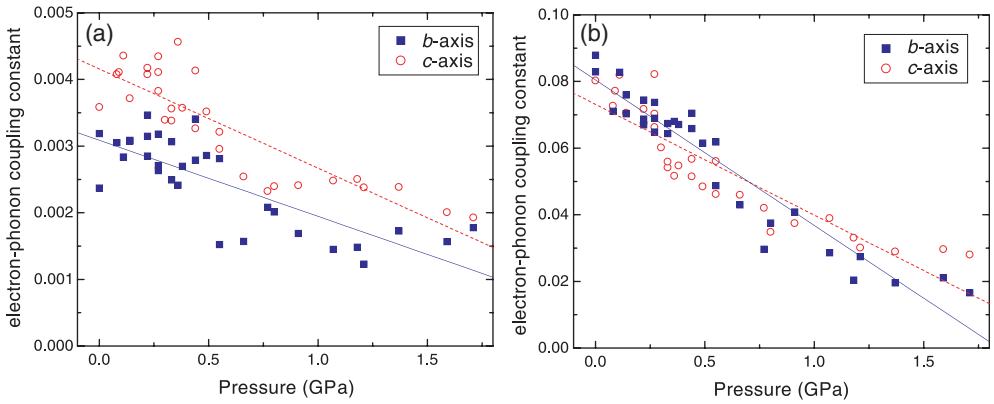

Figure 5. The pressure dependence of the electron–phonon coupling constant. Solid squares and lines are for polarization parallel to the *b*-axis while hollow circles and dashed lines are for polarization parallel to the *c*-axis. (a) For the C–S mode and (b) for the C=C mode.

electronic processes are subject to remormalization by many-body effects. In the following subsection we do not attempt to identify the origin of the renormalizations, but present evidence of their influence on the pressure dependence of the electronic contributions to the IR spectrum.

4.1. The pressure dependence of the carrier effective mass

This subsection focuses on the pressure dependence of the carrier effective mass extracted from modelling with the phase-phonon theory. The plasma frequency, ω_p, parameterizes the charge carrier density, $\mathcal{N}$, and effective mass, here denoted as m^*_{pp}:

$$\omega_p^2 = \frac{\mathcal{N}e^2}{\epsilon_0 m^*_{pp}}. \tag{25}$$

For our actual pressure range the band filling is independent of pressure and the carrier density only has a small pressure dependence arising from the reduction in unit cell parameters [2, 6].

For a plasma frequency dominated by intraband processes the pressure dependence of m^*_{pp} arises solely from the pressure dependence of the band parameters [5, 6], i.e. the increase in bandwidth and curvature as the wavefunction overlap increases. We argue that if the plasma frequency also parameterizes the interband processes, it will contain contributions from quasiparticle mass renormalization. The first point to note (see section 3.3) is that the plasma frequency in the phase-phonon model not only describes the screening ability of the free carriers (the intraband response) but also the density of states and band curvatures associated with intraband absorption. Thus, following the preceding logic, the mass m^*_{pp} will to some extent be renormalized by many-body effects [5].

The second point to note is that using the pressure dependence of the Raman modes to constrain the mode frequencies for the phase-phonon model significantly reduces the parameter space encountered when modelling the IR response of this system. This is not only because it eliminates the mode frequencies as free parameters, but because the softening of the modes is dependent upon the perturbation to the band gap, $\Delta - \Delta_0$. In this manner the mode frequencies provide a further constraint on the parameters describing the electronic response. The parameters describing the electronic response are thus believed to have greater validity than those obtained from a simple Drude–Lorentz fit [6].

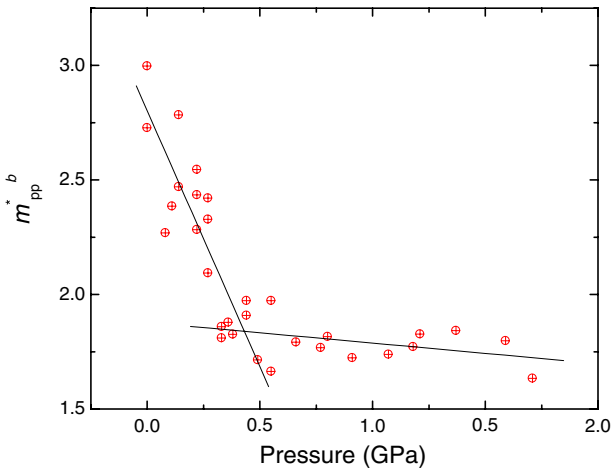

Figure 6. The mass m^{*b}_{pp} for light polarized parallel to the b-axis, deduced from the phase-phonon fit to the optical data. For $P < 0.5$ GPa, $\mathrm{d}m^{*b}_{pp}/\mathrm{d}P \sim -2.2\ m_e$ and $\mathrm{d}\ln m^{*b}_{pp}/\mathrm{d}P \sim -80\%\ \mathrm{GPa}^{-1}$. For $P > 0.5$ GPa, $\mathrm{d}m^{*b}_{pp}/\mathrm{d}P \sim -0.9\ m_e$ and $\mathrm{d}\ln m^{*b}_{pp}/\mathrm{d}P \sim -5\%\ \mathrm{GPa}^{-1}$.

The pressure dependence of the effective masses m^*_{pp} obtained using the phase-phonon theory is shown in figures 6 and 7. For both polarization directions, m^*_{pp} decreases with the application of pressure. For both polarizations this decrease is clearly non-linear and this is highlighted by linear fits to the low-pressure (<0.5 GPa) and high-pressure regions (>0.5 GPa) (see figures 6 and 7). These pressure ranges were chosen because the b-axis m^{*b}_{pp} clearly exhibits a change of slope at 0.5 GPa. The trend in m^{*c}_{pp} for polarization parallel to the c-axis is far less clear-cut. Band structure calculations giving the pressure dependence of the bare band mass [33] indicate a sublinear behaviour for its pressure dependence. However, this is a much smaller correction to linear behaviour than observed here and fails to reproduce the change in slope at 0.5 GPa. The coincidence of 'kinks' in the pressure dependence of m^*_{pp} obtained here and of m^* from magnetic quantum oscillation data [2] is thus an indication that the phase-phonon fitting procedure is sensitive to many-body effects. It is these renormalizations which are known to strongly influence superconductivity in this material [2, 6].

4.2. Implications for the superconducting pairing mechanism

It has been shown previously [34] that the usual electron–acoustic phonon interaction mechanism is unable to account for the magnitude of the electron–phonon coupling constant or the large pressure dependence of T_c in the BEDT-TTF superconductors. A further refinement [34] includes the attractive interaction mediated by the A_g molecular modes, with the total electron–phonon coupling constant, λ_{TOT}, given by a Yamaji sum over the individual A_g molecular modes. The energy scale for the interaction is set by the Debye frequency, Θ [34, 35]. Caulfield *et al* [2] have previously inferred $\Theta \approx 40\ \mathrm{cm}^{-1}$ by fitting the effective mass dependence of T_c with a linearized Eliashberg equation using an Einstein density of phonon states, $\delta(\Theta)$. High- and low-temperature specific heat measurements [36, 37] yield values of Θ ranging from 38 to 140 cm^{-1}. Calculations of λ_{TOT} [34] give values ranging from 0.25 to 0.45 [38–40].

The weak-coupling BCS formula [41] gives a satisfactory functional description of the ambient pressure T_c [8] and describes the effective mass dependence of the superconducting

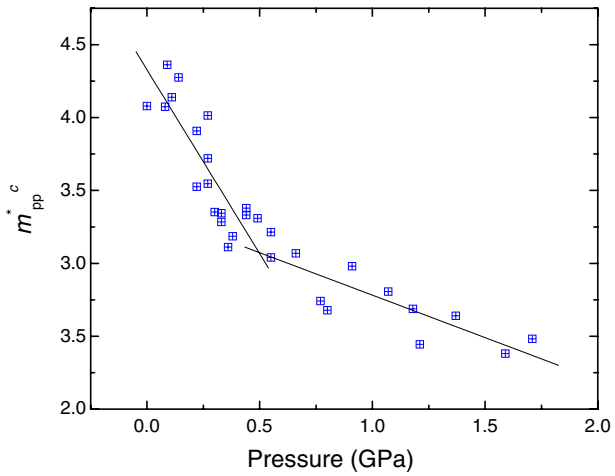

Figure 7. The mass m^{*c}_{pp} for light polarized parallel to the c-axis, deduced from the phase-phonon fit to the optical data. For $P < 0.5$ GPa, $dm^{*c}_{pp}/dP \sim -2.5\ m_e$ and $d \ln m^{*c}_{pp}/dP \sim -58\%$ GPa^{-1}. For $P > 0.5$ GPa, $dm^{*c}_{pp}/dP \sim -0.6\ m_e$ and $d \ln m^{*c}_{pp}/dP \sim -17\%$ GPa^{-1}.

transition temperature [2]. However, the fact that the weak-coupling BCS expression describes T_c versus m^* well [2] should NOT be taken to imply that κ-(BEDT-TTF)$_2$Cu(SCN)$_2$ is a weak-coupling BCS superconductor. The formula is used here as a convenient parameterization which is known to describe earlier data well [2, 42].

The pressure derivative of the weak-coupling BCS formula provides a convenient parameterization of $\frac{d \ln T_c}{dP}$ in terms of $\frac{d\lambda}{dP}$:

$$\frac{d \ln T_c}{dP} = \frac{d \ln \Theta}{dP} + \frac{1}{(\lambda - \mu^*)^2}\left[\frac{d\lambda}{dP} - \frac{d\mu^*}{dP}\right]. \tag{26}$$

With

$$\frac{1}{(\lambda - \mu^*)^2} = \left[\ln\left(\frac{T_c}{1.13\Theta}\right)\right]^2, \tag{27}$$

$\Theta \approx 90 \pm 50$ cm^{-1} [2, 36, 37] and, using the average pressure-induced stiffening of the Raman active lattice modes of $\approx$+13% GPa^{-1} [7] for $\frac{d \ln \Theta}{dP}$, the only unknown is the pressure dependence of the Coulomb pseudopotential, $\frac{d\mu^*}{dP}$. There is sufficient uncertainty in the calculations of μ^* that an accurate estimate for its pressure dependence cannot be made [43]. However, μ^* is known to scale with the density of states at the Fermi energy [43], which will decrease with the application of pressure [2]. Thus if μ^* is positive [39] it will decrease with pressure and omitting $\frac{d\mu^*}{dP}$ from equation (26) will result in an overestimate for the rate of suppression of T_c with pressure. A negative value of μ^* indicates that direct (non-phonon-mediated) electron–electron interactions are involved in the pairing [2, 43] which are not measured by these experiments. Consequently $\frac{d\mu^*}{dP}$ is ignored in equation (26).

Estimates for the pressure dependence of the electron–phonon coupling constant, based on the vibrations sampled and the two methods of calculation, are used to calculate the right-hand side of equation (26). It should be emphasized that the two models that we are employing to estimate the pressure dependence of the electron–phonon coupling constant lie at opposite limits of our sample's behaviour, the dimer charge-oscillation model being the limit of a localized electronic system and the phase-phonon model the limit of an itinerant system. A conclusion common to both methods of analysis should thus be a robust one.

4.2.1. $T_c(P)$ from the dimer charge-oscillation model. Employing the dimer charge model, λ_{TOT} is assumed to have a pressure dependence similar to that of the strongly coupled C=C mode, i.e. of the order of -17% GPa^{-1}, with an upper limit of -20% GPa^{-1} used in this calculation. This gives $\frac{d \ln T_c}{dP} \approx -40 \pm 32\%$ GPa^{-1}, which is far from the experimentally observed value of $\frac{d \ln T_c}{dP} \approx -200\%$ GPa^{-1} [2, 3].

As can be seen from (27), Θ scales logarithmically with the dependence of the pressure derivative of T_c on the pressure derivative of the coupling constant. Thus to obtain the observed rapid fall of T_c with pressure from only the decrease in the electron–phonon coupling constant requires Θ to be of the order of the C=C mode frequency, $\approx$1500 cm^{-1}. Such a value is inconsistent with the 10 K superconducting temperature and the unconventional isotope shift observed upon carbon substitution [44]. Thus, the electron–phonon coupling as extracted from the dimer charge-oscillation model cannot be the relevant parameter for superconductivity in our organic superconductor.

4.2.2. $T_c(P)$ from the phase-phonon model. The pressure dependence of the electron–phonon coupling constant derived from the phase-phonon model provides far less clear-cut results. In this case λ_{TOT} is assumed to have a pressure dependence of $-40 \pm 20\%$ GPa^{-1}, a value consistent with the phase-phonon calculation of λ for all observed modes. This gives $\frac{d \ln T_c}{dP} \approx -90\%$ GPa^{-1} with the asymmetric errors of +150 and -77% GPa^{-1}. The upper bound of this estimate is close to the experimentally observed value of $\frac{d \ln T_c}{dP} \approx -200\%$ GPa^{-1} [2, 3]. Thus, the upper estimate of all parameters would be required to explain the pressure dependence of $T_c(P)$ as arising solely due to a reduction in the electron–phonon coupling constant.

4.2.3. Comparison. Again, it should be stressed that the dimer charge-oscillation model represents the limit of localized electronic behaviour and the phase-phonon model represents the limit of itinerant electronic behaviour. The true properties of κ-(BEDT-TTF)$_2$Cu(SCN)$_2$ under these experimental conditions are believed to lie somewhere between these extremes. The two models lead to similar conclusions, i.e. $\frac{d \ln T_c}{dP}$ cannot be reproduced within weak-coupling BCS theory. The fact that similar conclusions are drawn whichever model is employed suggests that they are robust.

Use of the dimer charge-oscillation model casts considerable doubt on whether this material is a simple BCS superconductor, because the characteristic energy of the pairing interaction would have to be of the order of the highest-frequency molecular modes, a value inconsistent with the 10 K superconducting transition temperature. However, this conclusion must be treated with caution due to the numerous assumptions involved in applying this model of a localized system to the coupling between the molecular vibrations and delocalized conduction electrons. Doubt on whether this material is a simple BCS superconductor is also cast by the application of the phase-phonon model, because the upper estimate of all parameters is required to explain the experimentally observed suppression of T_c with pressure.

This indicates that electron–electron interaction may be playing a significant role in this material's superconducting mechanism. It is worth noting that there is mounting evidence in support of this conclusion. Both experimental [45, 46] and theoretical [47] studies predict that the superconducting order parameter in this material has an 'exotic' d-wave symmetry, a property predicted for a superconducting state whose pairing is mediated by spin fluctuations [47, 48], i.e. direct electron–electron interaction [1].

5. Conclusions

Comparison of high-pressure Raman scattering and IR reflectivity data provides an alternative method for probing the quasiparticle contributions to effective mass enhancement known to be intimately connected to superconductivity in this material [2]. It also enables the pressure dependence of the electron–phonon coupling strength to be evaluated for modes observed in both spectra. Using the weak-coupling limit of BCS theory, the pressure dependence of the electron–phonon coupling constant is compared to the pressure dependence of the superconducting transition temperature. This casts doubt on whether this material is a simple BCS superconductor, an indication that electron–electron interaction may be playing a significant role in this material's superconducting mechanism.

Acknowledgments

The authors would like to thank A P Jephcoat and H Olijnyk from the Earth Science Department, Oxford University, UK, and A F Goncharov, V V Struzhkin, Ho-kwang Mao and R J Hemley from the Geophysical Laboratory, Carnegie Institute, Washington, USA, for their stimulating collaboration that resulted in the measurements [6, 7] that the analysis in this paper is based upon. This work was supported by the EPSRC (UK).

References

[1] Singleton J 2000 *Rep. Prog. Phys.* **63** 1111
Singleton J and Mielke C H 2002 *Contemp. Phys.* **43** 63
[2] Caulfield J, Lubczynski W, Pratt F, Singleton J, Ko D, Hayes W, Kurmoo M and Day P 1994 *J. Phys.: Condens. Matter* **6** 2911
[3] Murata K, Honda Y, Anzai H, Tokumoto M, Takahashi K, Kinoshita M and Ishiguro T 1989 *Synth. Met.* **27** A263
[4] Harrison N, Caulfield J, Singleton J, Reinders P H P, Herlach F, Hayes W, Kurmoo M and Day P 1996 *J. Phys.: Condens. Matter* **8** 5415
[5] Leggett A 1968 *Ann. Phys., NY* **46** 76
[6] Klehe A-K, McDonald R, Goncharov A, Struzhkin V, Mao H, Hemley R, Sasaki T, Hayes W and Singleton J 2000 *J. Phys.: Condens. Matter* **12** L247
[7] McDonald R, Klehe A-K, Jephcoat A, Olijnyk H, Sasaki T, Hayes W and Singleton J 2001 *J. Phys.: Condens. Matter* **13** L291
[8] Sugano T, Hayashi H, Kinoshita M and Nishikida K 1989 *Phys. Rev.* B **39** 11387
[9] Kornelsen K, Eldridge J, Wang H and Williams J 1989 *Solid State Commun.* **72** 475
[10] Rice M 1979 *Solid State Commun.* **31** 93
[11] Eldridge J, Homes C, Williams J, Kini A and Wang H 1995 *Spectrochim. Acta* A **51** 947
[12] McDonald R, Klehe A-K, Singleton J and Hayes W 2003 *Synth. Met.* **133–134** 251
[13] Zallen R 1974 *Phys. Rev.* B **9** 4485
[14] Yartsev V and Graja A 1998 *Int. J. Mod. Phys.* B **12** 1643
[15] Rice M 1976 *Phys. Rev. Lett.* **37** 36
[16] Yartsev V and Graja A 1990 *J. Phys.: Condens. Matter* **2** 9631
[17] Rice M, Yartsev V M and Jacobsen C S 1979 *Phys. Rev.* B **21** 3437
[18] Bozio R, Meneghetti M and Pecile C 1982 *J. Chem. Phys.* **79** 5793
[19] Rice M, Pietronero L and Brüesch P 1977 *Solid State Commun.* **21** 757
[20] Kornelsen K, Eldridge J, Wang H and Williams J 1991 *Phys. Rev.* B **44** 5235
[21] Kozlov M and Tokumoto M 1995 *Synth. Met.* **70** 1023
[22] Inkson J 1984 *Many-Body Theory of Solids* (New York: Plenum)
[23] Haken H 1976 *Quantum Field Theory of Solids* (Amsterdam: North-Holland)
[24] Pines D and Nozières P 1966 *The Theory of Quantum Liquids* vol 1 (New York: Benjamin)
[25] Kubo R 1956 *Can. J. Phys.* **34** 1274
[26] Pines D 1962 *The Many-Body Problem* (New York: Benjamin)

[27] Painelli A, Girlando A and Pecile C 1984 *Solid State Commun.* **52** 801
[28] Dove M 1993 *Introduction to Lattice Dynamics* (Cambridge: Cambridge University Press)
[29] Lee P, Rice M and Anderson P 1974 *Solid State Commun.* **14** 703
[30] Fenton E and Psaltakis G C 1983 *Solid State Commun.* **47** 767
[31] Merino J and McKenzie R 1998 *Comment. Condens. Matter. Phys.* **18** 309
[32] Wang N, Clayman B, Mori H and Tanaka S 2000 *Physica* C **341** 2225
[33] McDonald R, Goddard P A and Singleton J 2002 at press
[34] Yamaji K 1986 *Solid State Commun.* **61** 413
[35] Faulhaber J, Ko D and Briddon P 1993 *Synth. Met.* **60** 227
[36] Fortune N, Rajaram G and Murata K 1999 *Synth. Met.* **103** 2080
[37] Andraka B, Kim J, Stewart G, Carlson K, Wang H and Williams J M 1998 *Phys. Rev.* B **40** R11345
[38] Hill S 1993 *Synth. Met.* **55–57** 2566
[39] Shumway J, Chattopadhyay S and Satpathy S 1996 *Phys. Rev.* B **53** 6677
[40] Drozdova O, Semkin V, Vlasova R, Kushch N and Yagubskii E 1994 *Synth. Met.* **64** 17
[41] Bardeen J, Cooper L and Schrieffer J 1957 *Phys. Rev.* **108** 1175
[42] Caulfield J, Lubczynski W, Lee W, Singleton J, Pratt F, Hayes W, Kurmoo M and Day P 1995 *Synth. Met.* **70** 185
[43] Lee W 1998 *Solid State Commun.* **106** 601
[44] Schlueter J, Kini A, Ward B, Geiser U, Wang H, Mohtasham J, Winter R and Gard G 2001 *Physica* C **351** 261
[45] Izawa K, Yamaguchi H, Sasaki T and Matsuda Y 2002 *Phys. Rev. Lett.* **88** 027002
[46] Arai T, Ichimura K, Takasaki S, Nakatsuji J Y S and Anzai H 2001 *Phys. Rev.* B **63** 104518
[47] Kuroki K, Kimura T, Arita R, Tanaka Y and Matsuda Y 2002 *Phys. Rev.* B 100516
[48] Annett J 1995 *Contemp. Phys.* **36** 423